
Markovian Gaussian Process: A Universal State-Space Representation for Stationary Temporal Gaussian Process

Weihan Li¹, Yule Wang¹, Chengrui Li¹, Anqi Wu^{1,*}

¹School of Computational Science & Engineering,
Georgia Institute of Technology, Atlanta, GA 30332,
weihanli@gatech.edu, yulewang@gatech.edu,
cnlichengrui@gatech.edu, anqiwu@gatech.edu

Abstract

Gaussian Processes (GPs) and Linear Dynamical Systems (LDSs) are essential time series and dynamic system modeling tools. GPs can handle complex, non-linear dynamics but are computationally demanding, while LDSs offer efficient computation but lack the expressive power of GPs. To combine their benefits, we introduce a universal method that allows an LDS to mirror stationary temporal GPs. This state-space representation, known as the Markovian Gaussian Process (Markovian GP), leverages the flexibility of kernel functions while maintaining efficient linear computation. Unlike existing GP-LDS conversion methods, which require separability for most multi-output kernels, our approach works universally for single- and multi-output stationary temporal kernels. We evaluate our method by computing covariance, performing regression tasks, and applying it to a neuroscience application, demonstrating that our method provides an accurate state-space representation for stationary temporal GPs.

1 Introduction

Gaussian Process (GP) and Linear Dynamical System (LDS) are foundational for modeling time series and dynamic systems across various scientific fields. In neuroscience, for instance, GPs are used to model latent representations of high-dimensional neural recordings [Yu et al., 2008; Wu et al., 2017], and LDSs are utilized to learn neural dynamics with switching states during decision-making [Zoltowski et al., 2020]. In climate science, GPs are employed to model spatio-temporal precipitation levels [Sarkka et al., 2013], and LDSs are used to monitor air pollution [Lippert et al., 2024].

These two approaches offer distinct advantages and limitations. One of the main strengths of GPs is their flexibility in modeling complex, non-linear temporal dynamics using different kernel functions. However, their computational cost is cubic, $\mathcal{O}(T^3)$, and their memory storage requirement is quadratic, $\mathcal{O}(T^2)$, in the number of samples T , which limits their application to large datasets. In contrast, LDSs have linear computational and memory costs, $\mathcal{O}(T)$, but lack the expressive power of GPs for representing temporal dynamics using various kernels.

Our objective is to leverage the benefits of both methodologies by developing an LDS that emulates a stationary temporal GP. This state-space representation of a GP is known as a Markovian Gaussian Process (Markovian GP) [Zhao, 2021; Zhu et al., 2023]. By adopting this approach, we can estimate model parameters following the Kalman Filter framework and perform time series regressions with the Kalman Filtering and Smoothing algorithm [Kailath et al., 2000]. Notably, both of these techniques have linear computational and memory costs.

*Corresponding authors: Anqi Wu

Table 1: Existing works for GP-LDS conversions.

Kernel	Paper	Technique	Exact conversion
Exponential, Matern, Squared Exponential	Hartikainen & Särkkä 2010	Spectral Factorization, Taylor Approximation.	Exponential, Matern
Rational Quadratic	Solin & Särkkä 2014b	Approximated by Squared Exponential.	No
Periodic	Solin & Särkkä 2014a	Taylor Approximation.	No
Spatio-Temporal, Multi-Output Matern, Multi-Output LMC	Solin et al. 2016, Sarkka et al. 2013	Spectral Factorization, Kronecker Product.	Multi-output Matern, LMC depends on the single-output kernel.

Existing Markovian GP methods have two limitations: (1) For multi-output kernels, they can only handle multi-output Matern kernel or kernels that are separable over spatial and temporal domains. Many multi-output kernels, such as the multi-output squared exponential kernel, are not compatible with current methods since they are non-separable, despite being commonly used in real-world applications, such as neuroscience [Gokcen et al., 2022] and environmental engineering [Parra & Tobar, 2017]. (2) The conversion processes differ across various kernels, requiring specialized techniques for each. For example, the Exponential kernel and Matern kernel have closed-form conversions. In contrast, the Squared Exponential kernel necessitates a Taylor series to approximate spectral density, and the Rational Quadratic kernel is approximated as a sum of Squared Exponential kernels [Solin et al., 2016].

This work presents a universal state-space representation method for stationary temporal kernels studied in the GP-LDS literature, including both single- and multi-output cases. Our method does not require specialized techniques for different kernels, and the resulting Markovian GPs can leverage the robust representational capabilities of kernel functions while maintaining linear computational costs over samples.

We first test our method on synthetic data by comparing estimated covariance and regression performance. Then, we evaluate our method’s ability to handle real-world time series regression tasks against GP and Sparse GP with inducing points [Matthews, 2017]. Finally, we apply our method to convert a GPFA-based model to an LDS within a neuroscience application [Gokcen et al., 2022].

2 Related Works

Markovian Gaussian Process. Several studies have explored the connections between Gaussian Processes and Linear Dynamical Systems (GP-LDS). Notably, in the context of GP-LDS conversion, all methods require the kernels to take a temporal input. A particular case is the spatio-temporal kernel [Sarkka et al., 2013], which has both a temporal and multi-dimensional spatial input. However, its LDS conversion occurs only in the temporal domain. We summarize existing Markovian GPs in Table 1, where most studies focus on single-output temporal kernels. For multi-output kernels, except for the multi-output Matern kernel, existing methods require kernel separability over spatial and temporal domains, such as spatio-temporal kernels or Linear Model of Coregionalization (LMC)-based kernels.

Regarding applications, Zhu et al. 2023 utilized a Markovian GP as the prior distribution in a variational autoencoder. Hamelijncck et al. 2021 employed a Spatio-Temporal Markovian GP to develop a scalable GP variational inference algorithm. Li et al. 2024 used a Markovian GP to discover latent communication between multiple brain regions.

Scalable Gaussian Process. In addition to the Markovian GPs mentioned earlier, various approaches have been introduced to enhance the scalability of GPs. Titsias 2009; Matthews 2017; Galy-Fajou & Oppet 2021 developed sparse GPs with inducing points, achieving a computational cost of $\mathcal{O}(Tm^2)$, where T and m are the number of samples and inducing points, respectively. Wang et al. 2019 proposed a parallel algorithm to scale exact GP inference on GPUs. Hensman et al. 2015 and Cheng & Boots 2017 utilized a set of learned variational parameters to approximate GP inference with minibatch training. In this work, our primary focus is to build a universal framework for the

connection to LDS, so we will not extensively compare Markovian GP with current scalable GP methods.

3 Method

To achieve a universal state-space representation of stationary temporal Gaussian Process (GP) with kernel \mathbf{K} , we first establish the connection between the GP's kernel function and the parameters of a Linear Dynamical System (LDS). We then develop a method that takes the kernels as input and generates the desired transition and measurement matrices, uniquely describing an LDS's dynamics.

Gaussian Process and State-Space Representation. We assume that an M dimensional stationary time series $\mathbf{X} = [x_1, \dots, x_T] \in \mathbb{R}^{M \times T}$ is modeled as a stationary Gaussian Process (GP):

$$\begin{bmatrix} x_1 \\ x_2 \\ \vdots \\ x_T \end{bmatrix} \sim \mathcal{GP}(0, \begin{bmatrix} \mathbf{K}(0) & \mathbf{K}(-1) & \dots & \mathbf{K}(-T+1) \\ \mathbf{K}(1) & \mathbf{K}(0) & \dots & \mathbf{K}(-T+2) \\ \vdots & \vdots & \ddots & \vdots \\ \mathbf{K}(T-1) & \mathbf{K}(T-2) & \dots & \mathbf{K}(0) \end{bmatrix}), \quad (1)$$

where $x_t \in \mathbb{R}^{M \times 1}$ is the observation sample at time t and each $\mathbf{K}(\tau) \in \mathbb{R}^{M \times M}$ is the kernel between two time points with an interval τ . Our objective is to find a state-space representation of \mathbf{X} , which follows a discrete-time linear dynamical system (LDS) structure:

$$x_t = \sum_{p=1}^P \mathbf{A}_p x_{t-p} + q_t, \quad q_t \sim \mathcal{N}(0, \mathbf{Q}), \quad (2)$$

where P represents the number of time lags, $\mathbf{A}_1, \dots, \mathbf{A}_P \in \mathbb{R}^{M \times M}$ are the transition matrices, and $\mathbf{Q} \in \mathbb{R}^{M \times M}$ is the measurement matrix.

Determining an LDS using Kernels. To estimate transition matrices and measurement using \mathbf{X} , we can consider the discrete-time LDS in Eq. 2 as a regression model [Neumaier & Schneider, 2001]:

$$x_t = \mathbf{G}v_t + q_t, \quad q_t \sim \mathcal{N}(0, \mathbf{Q}), \quad (3)$$

where $\mathbf{G} \in \mathbb{R}^{M \times MP}$ is the regression coefficient and $v_t \in \mathbb{R}^{MP \times 1}$ is the predictor:

$$\mathbf{G} = [\mathbf{A}_P, \mathbf{A}_{P-1}, \dots, \mathbf{A}_1], \quad v_t = [x_{t-P}^\top, x_{t-P+1}^\top, \dots, x_{t-1}^\top]^\top. \quad (4)$$

Our ultimate goal is to use \mathbf{K} to represent \mathbf{G} and \mathbf{Q} . First, we can represent \mathbf{G} and \mathbf{Q} as functions of \mathbf{X} . Concretely, given T samples, x_1, \dots, x_T , we define predictor matrix as $\mathbf{V} = [v_{P+1}, \dots, v_T]^\top \in \mathbb{R}^{MP \times (T-P)}$ and target observation matrix as $\mathbf{W} = [x_{P+1}, \dots, x_T] \in \mathbb{R}^{M \times (T-P)}$. Then, we can represent the regression model in Eq. 3 in the matrix form: $\mathbf{W} = \mathbf{G}\mathbf{V} + \mathbf{R}$, where \mathbf{R} is the residual matrix. By doing so, we can estimate coefficient matrix \mathbf{G} and the measurement matrix \mathbf{Q} by least squares estimation:

$$\mathbf{G} = \mathbf{W}\mathbf{V}^\top (\mathbf{V}\mathbf{V}^\top)^{-1}, \quad \mathbf{Q} = \frac{\mathbf{R}\mathbf{R}^\top}{T-P-1}, \quad (5)$$

where $\mathbf{R} = \mathbf{W} - \mathbf{G}\mathbf{V}$ denotes an estimate of the residual matrix, and its covariance is an estimate of measurement matrix \mathbf{Q} . Now, if we can represent $\mathbf{W}\mathbf{V}^\top$, $\mathbf{W}\mathbf{W}^\top$, and $\mathbf{V}\mathbf{V}^\top$ with \mathbf{K} , we will achieve the ultimate goal.

Let's inspect $\mathbf{V}\mathbf{V}^\top \in \mathbb{R}^{MP \times MP}$ first. We have:

$$\begin{aligned} \mathbf{V}\mathbf{V}^\top &= \begin{bmatrix} x_1 & x_2 & \dots & x_{T-P} \\ x_2 & x_3 & \dots & x_{T-P+1} \\ \vdots & \vdots & \ddots & \vdots \\ x_P & x_{P+1} & \dots & x_{T-1} \end{bmatrix} \begin{bmatrix} x_1^\top & x_2^\top & \dots & x_P^\top \\ x_2^\top & x_3^\top & \dots & x_{P+1}^\top \\ \vdots & \vdots & \ddots & \vdots \\ x_{T-P}^\top & x_{T-P+1}^\top & \dots & x_{T-1}^\top \end{bmatrix} \\ &= \begin{bmatrix} x_1x_1^\top + \dots + x_{T-P}x_{T-P}^\top & \dots & x_1x_P^\top + x_2x_{P+1}^\top + \dots + x_{T-P}x_{T-1}^\top \\ \vdots & \ddots & \vdots \\ x_Px_1^\top + \dots + x_{T-1}x_{T-P}^\top & \dots & x_Px_P^\top + x_{P+1}x_{P+1}^\top + \dots + x_{T-1}x_{T-1}^\top \end{bmatrix}, \end{aligned} \quad (6)$$

where the first element $x_1 x_1^\top \in \mathbb{R}^{M \times M}$ represents the auto-covariance of x_1 , which is essentially the kernel $\mathbf{K}(0)$ (Eq. 1). In other words, since \mathbf{X} is modeled as a stationary GP, the elements $x_1 x_1^\top, \dots, x_{T-1} x_{T-1}^\top$ are all equivalent and correspond to the diagonal elements $\mathbf{K}(0)$ in Eq. 1. Similarly, the elements $x_P x_1^\top, \dots, x_{T-1} x_{T-P}^\top$ represent cross-covariances with time interval $P-1$, which correspond to the off-diagonal elements $\mathbf{K}(P-1)$. Therefore, we can further write Eq. 6 as:

$$\begin{aligned} \mathbf{V}\mathbf{V}^\top &= \begin{bmatrix} \mathbf{K}(0) + \dots + \mathbf{K}(0) & \dots & \mathbf{K}(-P+1) + \dots + \mathbf{K}(-P+1) \\ \vdots & \ddots & \vdots \\ \mathbf{K}(P-1) + \dots + \mathbf{K}(P-1) & \dots & \mathbf{K}(0) + \dots + \mathbf{K}(0) \end{bmatrix} \\ &= (T-P) \cdot \begin{bmatrix} \mathbf{K}(0) & \mathbf{K}(-1) & \dots & \mathbf{K}(-P+1) \\ \mathbf{K}(1) & \mathbf{K}(0) & \dots & \mathbf{K}(-P+2) \\ \vdots & \vdots & \ddots & \vdots \\ \mathbf{K}(P-1) & \mathbf{K}(P-2) & \dots & \mathbf{K}(0) \end{bmatrix}. \end{aligned} \quad (7)$$

Following the same way, we can also represent $\mathbf{W}\mathbf{V}^\top \in \mathbb{R}^{M \times MP}$ and $\mathbf{W}\mathbf{W}^\top \in \mathbb{R}^{M \times M}$ using \mathbf{K} :

$$\begin{aligned} \mathbf{W}\mathbf{V}^\top &= (T-P) \cdot [\mathbf{K}(P) \quad \mathbf{K}(P-1) \quad \dots \quad \mathbf{K}(1)], \\ \mathbf{W}\mathbf{W}^\top &= (T-P) \cdot \mathbf{K}(0), \end{aligned} \quad (8)$$

Notably, each covariance $\mathbf{K}(\tau) \in \mathbb{R}^{M \times M}$, $\tau \in [-P+1, P-1]$ is only related to the feature dimension M of the observations and can be efficiently computed using the stationary kernel function employed in the GP. For example, single-output Squared Exponential kernel, $\mathbf{K}(\tau) = \sigma^2 \exp(-\frac{\tau^2}{2l^2}) \in \mathbb{R}^1$ with σ and l denoting the amplitude and length scale, or multi-output Spectral Mixture kernel [Parra & Tobar, 2017]:

$$\mathbf{K}(\tau) = \begin{bmatrix} \mathbf{K}_{11}(\tau) & \mathbf{K}_{12}(\tau) & \dots \\ \mathbf{K}_{21}(\tau) & \mathbf{K}_{22}(\tau) & \dots \\ \vdots & \vdots & \ddots \end{bmatrix} \in \mathbb{R}^{M \times M}, \quad (9)$$

where $\mathbf{K}_{ij}(\tau) = \sigma_{ij} \exp\left(-\frac{(\tau+\theta_{ij})^2}{2l_{ij}^2}\right) \cos((\tau+\theta_{ij})\omega_{ij} + \phi_{ij})$, with i and j denoting two channels, σ_{ij} , θ_{ij} , l_{ij} , ω_{ij} , and ϕ_{ij} representing amplitude, time delay, length scale, frequency, and phase delay.

In practice, we can denote $N = T - P$ as an amplitude coefficient. Note that N can be any value satisfying $N \geq P + 1$, which means performing the regression model in Eq. 4 using a group of sliding windows with a total N time samples. Moreover, the inverse of $\mathbf{V}\mathbf{V}^\top$ in Eq. 5 can sometimes have numerical issues, and a numerically stable approach is to use Cholesky factorization. See Appendix C for details.

Markovian Gaussian Process. Now, the transition matrices and the measurement matrix in Eq. 2 are uniquely determined by the kernel functions of GP by Eq. 5, Eq. 7 and Eq. 8, establishing a closed-form state-space mapping between a stationary temporal GP and a discrete-time LDS. Moreover, we can simplify the LDS in Eq. 2 to an LDS with a Markovian structure, resulting in a Markovian Gaussian Process (Markovian GP):

$$\hat{x}_t = \hat{\mathbf{A}}\hat{x}_{t-1} + q_t, \quad q_t \sim \mathcal{N}(0, \hat{\mathbf{Q}}), \quad x_t = \mathbf{H}\hat{x}_t, \quad (10)$$

where $\mathbf{H} \in \mathbb{R}^{M \times MP}$ denotes a mask matrix, $\hat{\mathbf{A}} \in \mathbb{R}^{MP \times MP}$ is structured as a controllable canonical form [Grewal & Andrews, 2014] and zeros are added to $\hat{\mathbf{Q}} \in \mathbb{R}^{MP \times MP}$ so it matches the shape of $\hat{\mathbf{A}}$:

$$\hat{\mathbf{A}} = \begin{bmatrix} \mathbf{A}_1 & \mathbf{A}_2 & \dots & \mathbf{A}_{P-1} & \mathbf{A}_P \\ \mathbf{I}_M & 0 & \dots & 0 & 0 \\ 0 & \mathbf{I}_M & \dots & 0 & 0 \\ 0 & 0 & \ddots & 0 & 0 \\ 0 & 0 & \dots & \mathbf{I}_M & 0 \end{bmatrix}, \quad \hat{\mathbf{Q}} = \begin{bmatrix} \mathbf{Q} & 0 \\ 0 & 0 \end{bmatrix}, \quad \mathbf{H} = [\mathbf{I}_M \quad 0], \quad (11)$$

with $\mathbf{I}_M \in \mathbb{R}^{M \times M}$ being an identity matrix. Notably, although we use a Markovian structure to represent a stationary GP, our method still incorporates information from multiple time lags. Finally, our Markovian GP conversion method has a similar representation form to existing works in Table 1, with the primary difference being how we compute $\mathbf{A}_1, \dots, \mathbf{A}_P$ using GP kernels. See Appendix D for more details.

4 Inference

We have built a Markovian Gaussian Process (Markovian GP) to model $X \in \mathbb{R}^{M \times T}$. However, in many real applications, we only have noisy observations, which are denoted as $Y \in \mathbb{R}^{M \times T}$. To account for noise in Y , we include a Gaussian noise term in Eq. 10:

$$\begin{aligned}\hat{x}_t &= \hat{\mathbf{A}}\hat{x}_{t-1} + q_t, & q_t &\sim \mathcal{N}(0, \hat{\mathbf{Q}}), \\ y_t &= \mathbf{H}\hat{x}_t + \epsilon_t, & \epsilon_t &\sim \mathcal{N}(0, \mathbf{C}).\end{aligned}\tag{12}$$

Eq. 12 is called a Kalman Filter model, where $\mathbf{C} \in \mathbb{R}^{M \times M}$ is a diagonal covariance matrix that is uncorrelated with $\hat{\mathbf{A}}$ and $\hat{\mathbf{Q}}$.

Parameter Setting. The model parameters Θ are the kernel parameters that form transition and measurement matrices $\hat{\mathbf{A}}$ and $\hat{\mathbf{Q}}$, and the noise parameter \mathbf{C} . Additionally, the hyperparameters include the number of time lags P and amplitude coefficient N (replaces $T - P$ in Eq. 7 and Eq. 8). For the following experiments, we choose P and N that have a small approximation error to the true GP kernels (see Section 5.1), noting that only P affects the computational complexity of our method.

Inference Algorithm. Typically, for the Kalman Filter model in Eq. 12, there are two inference approaches: Kalman Filter with maximum likelihood estimation (MLE) and Kalman Filter Expectation–Maximization (EM) [Kailath et al., 2000]. For regression tasks, Kalman Filter MLE suffices since we have a fixed \mathbf{H} . Conversely, if \mathbf{H} is a learnable projection matrix from a high-dimensional to a low-dimensional space and X is a latent representation of Y , the Kalman Filter Expectation–Maximization (EM) algorithm could provide better performance.

Kalman Filter MLE. Given X , our goal is to maximize the log-likelihood (LL) of Eq. 12:

$$LL(X, Y|\Theta) = -\frac{TM}{2} \log(2\pi) - \frac{1}{2} \sum_{t=1}^T \log(|\mathbf{C} + \mathbf{H}\hat{P}_t\mathbf{H}^\top|)\tag{13}$$

$$- \frac{1}{2} \sum_{t=1}^T (y_t - \mathbf{H}\hat{x}_t)^\top (\mathbf{C} + \mathbf{H}\hat{P}_t\mathbf{H}^\top)^{-1} (y_t - \mathbf{H}\hat{x}_t),\tag{14}$$

where $\hat{x}_t = \mathbb{E}[x_t|y_{1:t}]$ and $\hat{P}_t = \mathbb{E}[x_t^\top x_t|y_{1:t}]$ are computed by a forward passes known as Kalman Filtering algorithm [Boots, 2009].

Kalman Filter EM algorithm. An alternative choice is to estimate Θ following the EM framework. Given latent variables X and current parameters as Θ^k , we aim to compute the expected log-likelihood (E-step) and update the parameters Θ such that $Q(\Theta|\Theta^k)$ is maximized (M-step):

$$Q(\Theta|\Theta^k) = \mathbb{E}_{X \sim p(\cdot|Y, \Theta^k)}[LL(X, Y|\Theta)],\tag{15}$$

$$\Theta^{k+1} = \arg \max_{\Theta} Q(\Theta|\Theta^k),\tag{16}$$

where E-step is computed by forward/backward passes known as Kalman Filtering/Smoothing. See Appendix E for details.

Time Series Regression. One benefit of using a Markovian GP is the ability to perform time series regression tasks with linear computational and memory costs in the number of samples, whereas GP requires cubic time and quadratic memory costs.

Denote the training and testing sets as $(t_{\text{train}}, y_{\text{train}})$ and $(t_{\text{test}}, y_{\text{test}})$, respectively. The parameters Θ are estimated using the Kalman Filter MLE with the training set $(t_{\text{train}}, y_{\text{train}})$. We treat the testing set as missing data [Kailath et al., 2000], meaning that during the forward pass (Kalman Filtering), we compute the expectations of the latent variable $\mathbb{E}[x_t|y_{\text{train}, 1:t}]$ at each time t . But those $x_t, t \in t_{\text{test}}$ are computed without the ‘‘corrections’’ from the test observations y_{test} . Finally, the backward pass (Kalman Smoothing) smoothes $\mathbb{E}[x_t|y_{\text{train}, 1:t}]$ to obtain $\mathbb{E}[x_{1:T}|y_{\text{train}, 1:T}]$, where the test predictions are given by $\mathbf{H}\mathbb{E}[x_{t \in t_{\text{test}}}|y_{\text{train}, 1:T}]$.

Computational Complexity. The Kalman Filtering (forward pass) and Kalman Smoothing (backward pass) algorithms are all linear with time steps. Specifically, the computational costs are: (1) performing Kalman Filtering or Kalman Smoothing: $\mathcal{O}(T)$ for time, $\mathcal{O}(M^2P^2T)$ for memory, (2) computing log-likelihood: $\mathcal{O}(M^3)$ for time, $\mathcal{O}(M^2P^2T)$ for memory, (3) computing $\hat{\mathbf{A}}, \hat{\mathbf{Q}}$: $\mathcal{O}(M^3P^3)$ for time, $\mathcal{O}(M^2P^2)$ for memory.

5 Experiments

Kernels for Conversion. We select ten commonly used kernels to evaluate our Markovian-GP conversion method’s performance and to compare it with GP and existing conversion methods in Table 1.

- **Exponential (Exp):** Single-output with $\mathbf{K}(t, t') = \sigma^2 \exp\left(-\frac{|t-t'|}{l}\right)$.
- **Matern 3/2 (Matern):** Single-output with $\mathbf{K}(t, t') = \sigma^2 \left(1 + \frac{\sqrt{3}|t-t'|}{l}\right) \exp\left(-\frac{\sqrt{3}|t-t'|}{l}\right)$.
- **Squared Exponential (SE):** Single-output with $\mathbf{K}(t, t') = \sigma^2 \exp\left(-\frac{(t-t')^2}{2l^2}\right)$.
- **Rational Quadratic (RQ):** Single-output with $\mathbf{K}(t, t') = \sigma^2 \left(1 + \frac{(t-t')^2}{2\alpha l^2}\right)^{-\alpha}$.
- **Periodic:** Single-output with $\mathbf{K}(t, t') = \sigma^2 \exp\left(-\frac{2 \sin^2\left(\frac{\omega|t-t'|}{2}\right)}{l^2}\right)$.
- **Spectral Mixture (SM) [Wilson & Adams, 2013]:** Single-output with $\mathbf{K}(t, t') = \sum_{q=1}^Q \sigma_q^2 \exp\left(-\frac{(t-t')^2}{2l_q^2}\right) \cos(\omega_q(t-t'))$.
- **Multi-Output Squared Exponential (MOSE) [Gokcen et al., 2022]:** Multi-output with $\mathbf{K}_{ij}(t, t') = \sigma_{ij}^2 \exp\left(-\frac{(t-t'+\delta_{ij})^2}{2l_{ij}^2}\right)$.
- **Multi-Output Spectral Mixture (MOSM) [Parra & Tobar, 2017]:** Multi-output with $\mathbf{K}_{ij}(t, t') = \sum_{q=1}^Q \sigma_{ij,q}^2 \exp\left(-\frac{(t-t'+\delta_{ij,q})^2}{2l_{ij,q}^2}\right) \cos(\omega_{ij,q}(t-t') + \phi_{ij,q})$.
- **Cross-Spectral Mixture (CSM) [Ulrich et al., 2015]:** Multi-output with $\mathbf{K}_{ij}(t, t') = \sum_{q=1}^Q \sum_{r=1}^R \sigma_{i,q}^r \sigma_{j,q}^r \exp\left(-\frac{(t-t')^2}{2l_{ij,q}^2}\right) \cos(\omega_{ij,q}(t-t') + \phi_{ij,q}^r)$.
- **Linear Model of Coregionalization (LMC):** Multi-output with $\mathbf{K}(t, t') = \sum_{q=1}^Q B_q \otimes k_q(t, t')$, where B_q is a coregionalization matrix and $k_q(t, t')$ is a single-output kernel.

In the kernels mentioned above, σ represents the amplitude, l denotes the length scale, α is the shape parameter controlling the smoothness, ω represents the angular frequency, and δ and ϕ are the time/phase delays between two channels.

5.1 Synthetic Experiment

We denote current GP-LDS conversion methods as M-GP-SF since they are primarily based on Spectral Factorization [Sayed & Kailath, 2001]. This section aims to compare our Markovian GP (M-GP), M-GP-SF, and GP from two perspectives: (1) comparing the covariance of our method’s samples to the covariance of samples from both GPs and M-GP-SF, and (2) measuring the quality of the state-space representation by evaluating regression performance with parameters fixed to true values.

Comparing Covariance. For each of the ten kernels mentioned above, we generate samples from GP, M-GP (by Eq. 10), and M-GP-SF (by Eq. 10). See Figure 2 in Appendix A for an example of samples. Finally, for each class of samples, we calculate the covariance and the mean squared error (MSE) between the computed covariance and the ground truth kernel matrix.

For kernels that require approximation [Zhao, 2021], such as the SE and RQ kernels, we set P and N (replacing $T - P$ in Eq. 7 and Eq. 8) to minimize the MSE while balancing the computational cost. Specifically, we choose P and N values that represent the "turning point" of the MSE curve. See an example in Figure 3 in Appendix A

For kernels that have an exact conversion using M-GP-SF, such as the Exp and Matern kernels, we set the time lags P to match our transition matrix in Eq. 12 to the transition matrix derived from M-GP-SF. Then, given P , we set the amplitude coefficient N by the same strategy mentioned above. In summary, the largest lag is $P = 8$ for the SE and RQ kernels, and the smallest lag is $P = 1$ for the Exp kernel, indicating an efficient state-space representation by our method. See Appendix F for detailed values and kernel parameter settings.

Table 2 and Table 3 present the covariance comparison results, where $k_q(t, t')$ in LMC is set to be an SE kernel. For all ten kernels except the Periodic kernel, our method’s covariance closely matches the GP’s covariance, indicating an accurate state-space representation. For the Periodic kernel, our

Table 2: Comparison of covariance and regression performance for six single-output kernels. The metrics include MSE between the covariance of samples and the ground truth kernel matrix and MSE and nLL for regression performance (lower values indicate better performance). Results are averaged over five random train/test splits. “—” indicates that the method for the kernel does not exist.

Cov-MSE / 10^{-2}	Exp	Matern 3/2	SE	RQ	Periodic	SM
GP	7.8 ± 0.1	7.0 ± 0.3	4.6 ± 0.4	5.4 ± 0.4	0.1 ± 0.1	1.5 ± 0.2
M-GP-SF	8.1 ± 0.2	7.2 ± 0.3	5.4 ± 0.5	5.6 ± 0.6	1.3 ± 0.3	—
M-GP	7.9 ± 0.2	7.0 ± 0.1	5.3 ± 0.5	5.4 ± 0.2	2.8 ± 0.5	1.4 ± 0.1
Reg-MSE / 10^{-1}	Exp	Matern 3/2	SE	RQ	Periodic	SM
GP	5.7 ± 0.1	5.9 ± 0.2	3.1 ± 0.1	3.0 ± 0.1	17.8 ± 0.1	3.0 ± 0.2
M-GP-SF	5.8 ± 0.1	6.2 ± 0.1	3.4 ± 0.1	3.1 ± 0.1	20.5 ± 0.4	—
M-GP	5.9 ± 0.1	6.2 ± 0.1	3.3 ± 0.1	3.4 ± 0.1	2.8 ± 0.1	3.3 ± 0.2
Reg-NLL / 10^3	Exp	Matern 3/2	SE	RQ	Periodic	SM
GP	6.5 ± 0.01	6.1 ± 0.01	7.1 ± 0.03	7.0 ± 0.03	11.2 ± 0.08	9.8 ± 0.07
M-GP-SF	6.1 ± 0.02	5.8 ± 0.02	6.3 ± 0.05	7.1 ± 0.02	11.6 ± 0.10	—
M-GP	6.3 ± 0.02	5.9 ± 0.02	6.8 ± 0.02	7.0 ± 0.01	6.4 ± 0.01	9.4 ± 0.02

Table 3: Comparison of covariance and regression performance for four multi-output kernels. The metrics include MSE between the covariance of samples and the ground truth kernel matrix and MSE and nLL for regression performance (lower values indicate better performance). Results are averaged over five random train/test splits. “—” indicates that the method for the kernel does not exist.

Cov-MSE / 10^{-2}	MOSE	MOSM	CSM	LMC
GP	6.5 ± 0.30	1.0 ± 0.20	1.0 ± 0.30	6.1 ± 0.40
M-GP-SF	—	—	—	6.8 ± 0.30
M-GP	7.4 ± 0.30	1.1 ± 0.10	1.1 ± 0.10	6.5 ± 0.40
Reg-MSE / 10^{-1}	MOSE	MOSM	CSM	LMC
GP	7.4 ± 0.02	7.5 ± 0.02	8.2 ± 0.05	0.66 ± 0.02
M-GP-SF	—	—	—	0.75 ± 0.02
M-GP	7.6 ± 0.04	7.9 ± 0.08	7.7 ± 0.09	0.72 ± 0.02
Reg-NLL / 10^3	MOSE	MOSM	CSM	LMC
GP	11.7 ± 0.02	12.5 ± 0.02	14.6 ± 0.08	14.9 ± 0.06
M-GP-SF	—	—	—	17.2 ± 0.05
M-GP	12.9 ± 0.01	14.2 ± 0.03	13.7 ± 0.03	15.1 ± 0.01

method and M-GP-SF show a relatively large discrepancy compared to the GP. One possible reason is that the Periodic kernel generates a purely oscillatory signal, which may not be well-captured by an LDS.

Measuring Regression performance. We generate samples with 300 points from a GP for each kernel with added Gaussian noise as the regression data. Then, we randomly split the samples into training $(t_{\text{train}}, y_{\text{train}})$ and testing sets $(t_{\text{test}}, y_{\text{test}})$ by 60% and 40%, respectively. Following the settings in [Hartikainen & Särkkä \[2010\]](#), all parameters are fixed to their true values to ensure a fair evaluation of the Markovian representation. Finally, to perform regression by LDS, we consider the testing set as missing data and use the Kalman Filtering/Smoothing to process the training set, while predicting y_{test} at the missing time steps t_{test} . See Section 4 for details.

Tables 2 and 3 present the regression comparison results. For most kernels, our method demonstrates regression performance comparable to GP and M-GP-SF in terms of MSE and negative log-likelihood (nLL). However, our method significantly outperforms both GP and M-GP-SF for the Periodic kernel, which contradicts the covariance comparison results. One possible reason is that the additional

Table 4: Comparison of regression performance on PM₁₀ data. The metrics include MSE, nLL, and training time (lower values are better). Results are averaged over five independent runs.

Reg	Test MSE / 10^{-2} ↓	Test NLL / 10^3 ↓	Time / min ↓
GP	3.0 ± 0.29	-1.08 ± 0.07	10.3 ± 0.04
SGPR-100	8.5 ± 0.15	1.46 ± 0.08	9.2 ± 0.05
SGPR-1000	4.2 ± 0.12	-0.40 ± 0.03	10.1 ± 0.02
SGPR-2000	6.0 ± 0.22	0.09 ± 0.06	13.8 ± 0.02
M-GP	3.6 ± 0.10	-0.84 ± 0.06	5.5 ± 0.07

observation noise disrupts the purely oscillatory nature of the kernel, and our method’s inaccurate approximation might better capture this noise.

5.2 Regression for Air Quality

This section aims to compare the regression performance of our Markovian GP conversion method on real-world time series data against standard GP and Sparse GP with inducing points.

Experimental Setup. We use the PM₁₀ data from the London Air Quality Network². The recorded data show periodic fluctuations and highly irregular behavior caused by events such as weather changes and traffic jams. We select hourly data from January 2020 to July 2020 from sensors within the downtown London area, resulting in a time series $Y \in \mathbb{R}^{4500 \times 15}$, where $T = 4500$ and $M = 15$. The dataset is split into training and testing sets using an 80%/20% random split.

We compare our method with GP regression and Sparse GP regression (SGPR) using 100, 1000, and 2000 inducing points, both implemented using GPyTorch [Gardner et al., 2018]. The parameters of our Markovian GP are inferred using Kalman Filter MLE. We use an LMC multi-output kernel for both methods, with $k_q(t, t')$ being the single-output Spectral Mixture (SM) kernel to capture periodic features. We set $P = 2$ and $N = 2$ following the strategy in Section 5.1. See Appendix G for hyperparameter setting and other training details.

Results. Table 4 presents the regression comparisons. Our method achieves a comparable MSE with GP, while significantly outperforming SGPR with 100, 2000 inducing points. In terms of nLL, our method also closely matches GP and is better than all SGPRs. Additionally, our method has the fastest training time (CPU), whereas SGPR does not show a significant efficiency advantage over GP. One explanation is that SGPR in GPyTorch actually has an $\mathcal{O}(T^2M^2)$ memory cost, which becomes the primary bottleneck in this dataset. Moreover, SGPR requires estimating the positions of inducing points, leading to a high computational cost; for example, SGPR with 2000 inducing points is slightly slower than GP.

Figure 4 in Appendix A shows the MSE, negative LL, and training time of our method for $P = 1, 2, 4, 6, 8$ with a fixed $N = 2$. The results indicate that, for the LMC with an SM kernel on this dataset, the MSE and training time exhibit a linear relationship with P . Additionally, Figure 5 in Appendix A shows the MSE, nLL, and training time of our method for $N = 2, 4, 6, 8, 10$ with a fixed $P = 2$, where a smaller N results in better performance.

5.3 Learning Neural Latent Representation

This section aims to explore the capability of our Markovian GP conversion method in a neuroscience application, where we convert a Gaussian Process Factor Analysis (GPFA) model to an LDS, achieving comparable performance with significantly improved efficiency.

Experimental Setup. Gokcen et al. 2022 proposed a GPFA-based model called DLAG to model the latent interactions between multiple brain regions. They use a multi-output Squared Exponential (MOSE) kernel with a time delay parameter δ_{ij} to discover the directional interactions between a monkey’s primary visual area (V1) and secondary visual cortex (V2). If a positive δ_{ij} is learned, it indicates a signal from V1 to V2, and vice versa. DLAG has a computational complexity of $\mathcal{O}(T^3D^3)$ and a memory cost of $\mathcal{O}(T^2D^2)$, where T, D are the number of time samples and latent variables.

²<https://www.londonair.org.uk/>

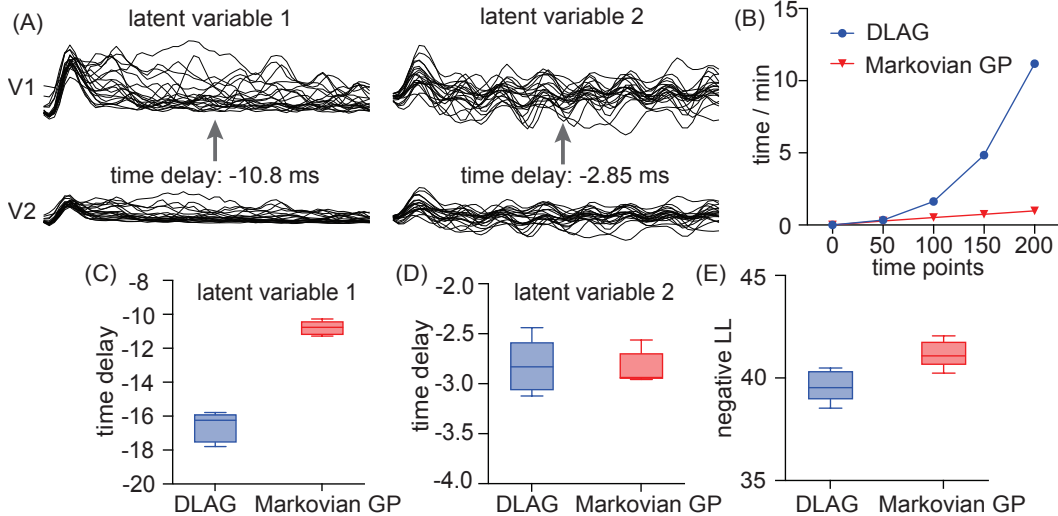


Figure 1: (A). Two pairs of latent variables are learned from V1 and V2 (20 trials are shown). For each pair of latent variables, there is a feedback signal from V2 to V1. (B). Comparison of time cost shows that the Markovian GP is significantly faster than DLAG. (C-D). Comparison of learned time delays indicates that the Markovian GP captures the same directional information as DLAG. (E). Comparison of negative LL shows that the Markovian GP closely matches DLAG.

We use neural spike train data from V1 and V2 [Semedo et al., 2019] with a 3:1 random training/test split. Following the settings in DLAG, we set the number of latent variables to $D = 8$, with four for V1 and four for V2. The first dimensions of V1 and V2 are modeled together as a two-output GP with a MOSE kernel, where the time delay parameter δ_{ij} captures the signal flow between V1 and V2. Similarly, the second dimensions of V1 and V2 are modeled together as a two-output GP with a MOSE kernel. In contrast, the third and fourth dimensions of V1 and V2 are modeled independently as four single-output GPs with SE kernels to capture region-specific information in the brain. See Appendix H for more details about DLAG and Appendix G for training details.

Besides, a state-space DLAG representation has the following structure:

$$\begin{aligned}\bar{x}_t &= \bar{\mathbf{A}}\bar{x}_{t-1} + q_t, & q_t &\sim \mathcal{N}(0, \bar{\mathbf{Q}}), \\ y_t &= \mathbf{L}\mathbf{H}\bar{x}_t + \epsilon_t, & \epsilon_t &\sim \mathcal{N}(0, \mathbf{C}),\end{aligned}\tag{17}$$

where $\bar{x}_t \in \mathbb{R}^{DP \times 1}$, $\mathbf{L} \in \mathbb{R}^{M \times D}$ is a projection matrix from high-dimensional neural data to a low-dimensional latent representation. We estimate the model parameters by Kalman Filter EM.

Results. Figure 1(A) displays the four learned latent variables from our method (20 trials are shown). The first row corresponds to V1, and the second corresponds to V2. Our method identifies two feedback signals from V2 to V1, consistent with the directional information of DLAG based on the learned delays δ_{ij} in Figure 1(C-D). Although the estimated delays do not have the same values, this does not affect the scientific conclusions, as the sign of the delays is more critical in neuroscience, and the differences in values are acceptable. In terms of negative LL, our method demonstrates comparable performance to DLAG (Figure 1(E)). Lastly, Figure 1(B) illustrates the time cost comparison, showing that our method significantly improves efficiency.

6 Discussion and Limitations

We propose a universal state-space representation for stationary temporal GP, resulting in a Markovian GP, which leverages the robust representational ability of kernels while maintaining linear computational costs over samples. We evaluate our Markovian GP from three perspectives: (1) covariance of generated samples, (2) regression performance, and (3) application to a GPFA model.

The limitations of our Markovian GP are twofold: (1) it is restricted to temporal inputs, with spatio-temporal inputs being a particular case since its LDS conversion occurs only in the temporal domain, and (2) it is limited to stationary GPs, as the derivation in Eq. 7 does not hold for non-stationary GPs.

References

- Boots, B. Learning stable linear dynamical systems. *Online*. Avail.: https://www.ml.cmu.edu/research/dap-papers/dap_boots.pdf [Accessed 30 05 2016], 2009.
- Cheng, C.-A. and Boots, B. Variational inference for gaussian process models with linear complexity. *Advances in Neural Information Processing Systems*, 30, 2017.
- Galy-Fajou, T. and Oppel, M. Adaptive inducing points selection for gaussian processes. *arXiv preprint arXiv:2107.10066*, 2021.
- Gardner, J., Pleiss, G., Weinberger, K. Q., Bindel, D., and Wilson, A. G. Gpytorch: Blackbox matrix-matrix gaussian process inference with gpu acceleration. *Advances in neural information processing systems*, 31, 2018.
- Gokcen, E., Jasper, A. I., Semedo, J. D., Zandvakili, A., Kohn, A., Machens, C. K., and Yu, B. M. Disentangling the flow of signals between populations of neurons. *Nature Computational Science*, 2(8):512–525, 2022.
- Grewal, M. S. and Andrews, A. P. *Kalman filtering: Theory and Practice with MATLAB*. John Wiley & Sons, 2014.
- Hamelijnck, O., Wilkinson, W., Loppi, N., Solin, A., and Damoulas, T. Spatio-temporal variational gaussian processes. *Advances in Neural Information Processing Systems*, 34:23621–23633, 2021.
- Hartikainen, J. and Särkkä, S. Kalman filtering and smoothing solutions to temporal gaussian process regression models. In *2010 IEEE international workshop on machine learning for signal processing*, pp. 379–384. IEEE, 2010.
- Hensman, J., Matthews, A., and Ghahramani, Z. Scalable variational gaussian process classification. In *Artificial Intelligence and Statistics*, pp. 351–360. PMLR, 2015.
- Kailath, T., Sayed, A. H., and Hassibi, B. *Linear estimation*. Number BOOK. Prentice Hall, 2000.
- Li, W., Li, C., Wang, Y., and Wu, A. Multi-region markovian gaussian process: An efficient method to discover directional communications across multiple brain regions. *arXiv preprint arXiv:2402.02686*, 2024.
- Lippert, F., Kranstauber, B., van Loon, E., and Forré, P. Deep gaussian markov random fields for graph-structured dynamical systems. *Advances in Neural Information Processing Systems*, 36, 2024.
- Matthews, A. G. d. G. *Scalable Gaussian process inference using variational methods*. PhD thesis, 2017.
- Neumaier, A. and Schneider, T. Estimation of parameters and eigenmodes of multivariate autoregressive models. *ACM Transactions on Mathematical Software (TOMS)*, 27(1):27–57, 2001.
- Parra, G. and Tobar, F. Spectral mixture kernels for multi-output gaussian processes. *Advances in Neural Information Processing Systems*, 30, 2017.
- Sarkka, S., Solin, A., and Hartikainen, J. Spatiotemporal learning via infinite-dimensional bayesian filtering and smoothing: A look at gaussian process regression through kalman filtering. *IEEE Signal Processing Magazine*, 30(4):51–61, 2013.
- Sayed, A. H. and Kailath, T. A survey of spectral factorization methods. *Numerical linear algebra with applications*, 8(6-7):467–496, 2001.
- Semedo, J. D., Zandvakili, A., Machens, C. K., Byron, M. Y., and Kohn, A. Cortical areas interact through a communication subspace. *Neuron*, 102(1):249–259, 2019.
- Solin, A. and Särkkä, S. Explicit link between periodic covariance functions and state space models. In *Artificial Intelligence and Statistics*, pp. 904–912. PMLR, 2014a.

- Solin, A. and Särkkä, S. Gaussian quadratures for state space approximation of scale mixtures of squared exponential covariance functions. In *2014 IEEE International Workshop on Machine Learning for Signal Processing (MLSP)*, pp. 1–6. IEEE, 2014b.
- Solin, A. et al. Stochastic differential equation methods for spatio-temporal gaussian process regression. 2016.
- Titsias, M. Variational learning of inducing variables in sparse gaussian processes. In *Artificial intelligence and statistics*, pp. 567–574. PMLR, 2009.
- Ulrich, K. R., Carlson, D. E., Dzirasa, K., and Carin, L. Gp kernels for cross-spectrum analysis. *Advances in neural information processing systems*, 28, 2015.
- Wang, K., Pleiss, G., Gardner, J., Tyree, S., Weinberger, K. Q., and Wilson, A. G. Exact gaussian processes on a million data points. *Advances in neural information processing systems*, 32, 2019.
- Wilson, A. and Adams, R. Gaussian process kernels for pattern discovery and extrapolation. In *International conference on machine learning*, pp. 1067–1075. PMLR, 2013.
- Wu, A., Roy, N. A., Keeley, S., and Pillow, J. W. Gaussian process based nonlinear latent structure discovery in multivariate spike train data. *Advances in neural information processing systems*, 30, 2017.
- Yu, B. M., Cunningham, J. P., Santhanam, G., Ryu, S., Shenoy, K. V., and Sahani, M. Gaussian-process factor analysis for low-dimensional single-trial analysis of neural population activity. *Advances in neural information processing systems*, 21, 2008.
- Zhao, Z. State-space deep gaussian processes with applications. *arXiv preprint arXiv:2111.12604*, 2021.
- Zhu, H., Balsells-Rodas, C., and Li, Y. Markovian gaussian process variational autoencoders. In *International Conference on Machine Learning*, pp. 42938–42961. PMLR, 2023.
- Zoltowski, D., Pillow, J., and Linderman, S. A general recurrent state space framework for modeling neural dynamics during decision-making. In *International Conference on Machine Learning*, pp. 11680–11691. PMLR, 2020.

A Additional Figures

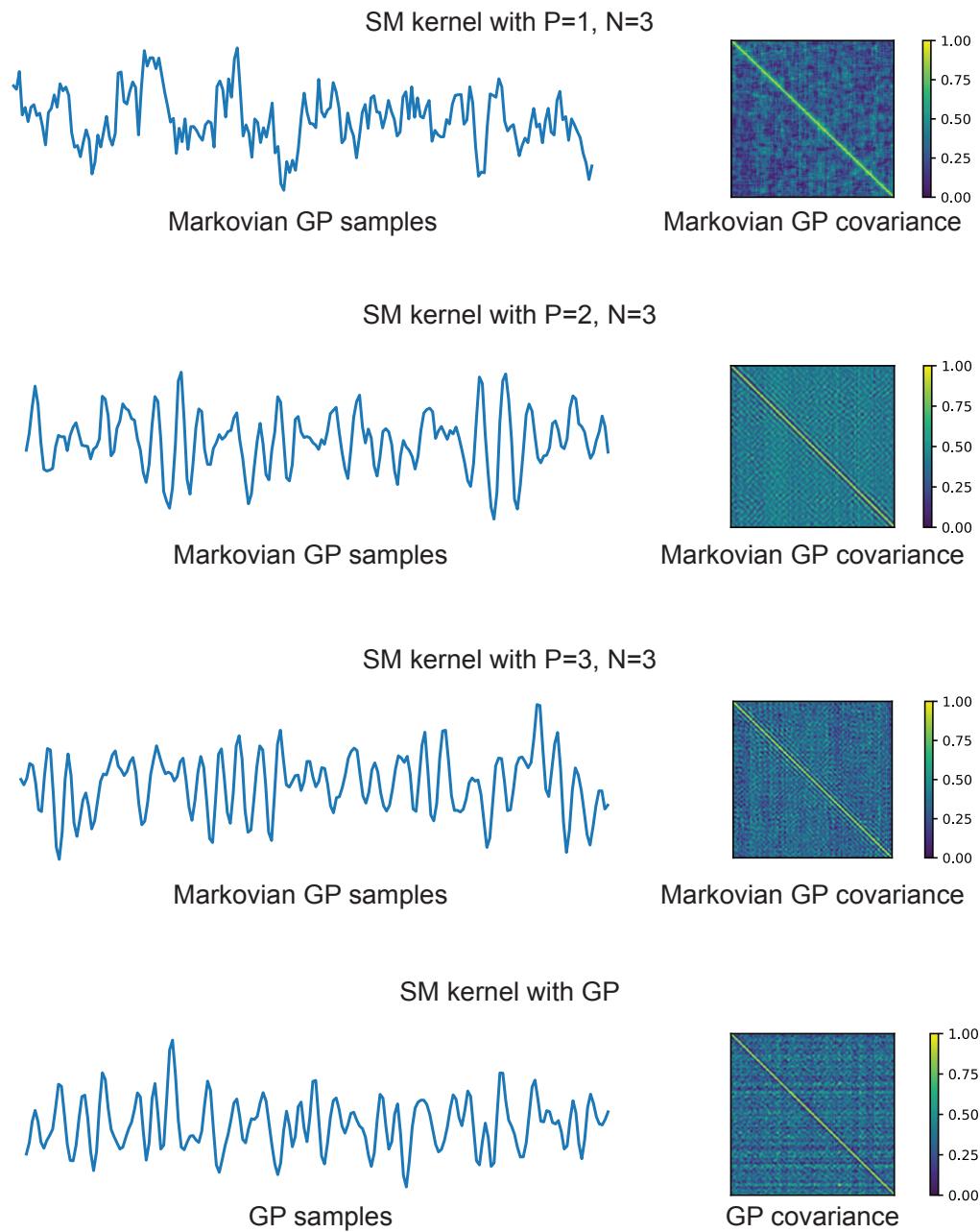


Figure 2: Visualize the samples from Markovian GP with $P = 1, 2, 3$ and GP. The results show that a smaller P will make the sample unsmooth.

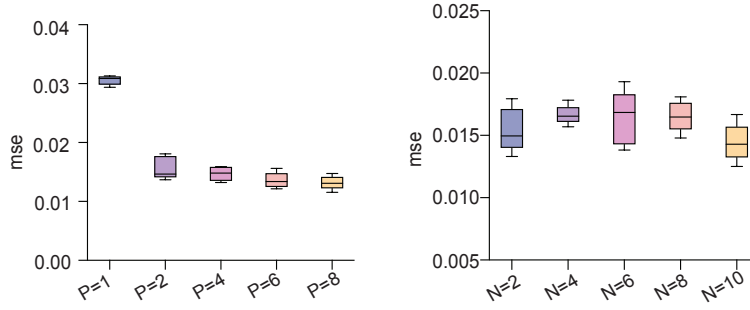


Figure 3: The MSE between the covariance of Markovian samples and the ground truth Spectral Mixture (SM) kernel is evaluated for two scenarios: (1) varying P values of 1, 2, 4, 6, and 8 with $N = 2$, and (2) varying N values of 2, 4, 6, 8, and 10 with $P = 2$. The results indicate that $P = 2$ represents a turning point for the covariance MSE, as illustrated by the samples in Figure 2. Additionally, the value of N does not have a significant effect on the covariance MSE.

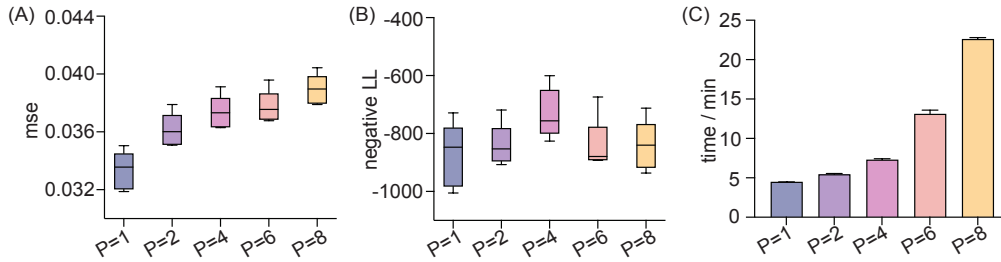


Figure 4: (A-C). The MSE, negative LL, and training time of the Markovian GP on the air quality regression task are evaluated for $P = 1, 2, 4, 6, 8$ with a fixed $N = 2$. The results show that the MSE and training time exhibit a linear relationship with P , whereas the negative LL does not. Note that $P = 1$ leads to unsmoothed samples for the SM kernel, as shown in Figure 2. The reason $P = 1$ gives a lower MSE is that the air quality data is highly unsmooth, making $P = 1$ perform better than $P = 2, 4, 6, 8$.

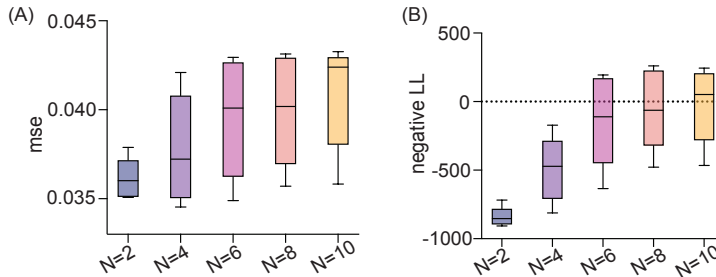


Figure 5: (A-B). The MSE, negative LL, and training time of the Markovian GP on the air quality regression task are evaluated for $M = 2, 4, 6, 8, 10$ with a fixed $P = 2$. The results show that the MSE and training time exhibit a linear relationship with N , but the variance increases as N enlarges. Recall that N replaces $T - P$; thus, the larger N is, the smaller Q in Eq. 5 becomes. A small Q may cause numerical problems when inverting Q during inference.

B Broader Impacts

The development of the Markovian Gaussian Process (Markovian GP) offers significant advancements in time series and dynamic system modeling. This method addresses a critical gap in existing modeling techniques by merging the computational efficiency of Linear Dynamical Systems (LDSs) with the expressive power of Gaussian Processes (GPs). This innovation can potentially impact various scientific and engineering domains where modeling complex, nonlinear time series is essential.

C Numerically Stable Computation

If the computation of \mathbf{G} in Eq.5 leads to numerical issues because $\mathbf{V}\mathbf{V}^\top$ has singular values that are nearly zero, a more numerically stable approach is to rewrite $\mathbf{V}\mathbf{V}^\top$ by Cholesky factorization:

$$\mathbf{D} = \begin{bmatrix} \mathbf{V}\mathbf{V}^\top & \mathbf{V}\mathbf{W}^\top \\ \mathbf{W}\mathbf{V}^\top & \mathbf{W}\mathbf{W}^\top \end{bmatrix} = \mathbf{L}\mathbf{L}^\top, \quad \mathbf{L} = \begin{bmatrix} \mathbf{L}_1 & 0 \\ \mathbf{L}_2 & \mathbf{L}_3 \end{bmatrix}, \quad \mathbf{V}\mathbf{V}^\top = \mathbf{L}_1\mathbf{L}_1^\top, \quad (18)$$

where $\mathbf{D} \in \mathbb{R}^{M(P+1) \times M(P+1)}$, $\mathbf{W}\mathbf{V}^\top = \mathbf{L}_2\mathbf{L}_1^\top$, $\mathbf{W}\mathbf{W}^\top = (T - P) \cdot \mathbf{K}(0)$, and $\mathbf{L}_1 \in \mathbb{R}^{MP \times MP}$, $\mathbf{L}_2 \in \mathbb{R}^{M \times MP}$, $\mathbf{L}_3 \in \mathbb{R}^{M \times M}$ are the sub-matrices of \mathbf{L} . In practice, Eq. 18 factorizes $\mathbf{D} + \delta\mathbf{I}$ with a small positive number δ to ensure the positive definite of \mathbf{D} . Then, the estimation for \mathbf{G} can be cast in the form of \mathbf{L} and the measurement matrix \mathbf{Q} is the residual covariance of residual \mathbf{R} :

$$\begin{aligned} \hat{\mathbf{G}} &= \mathbf{W}\mathbf{V}^\top(\mathbf{V}\mathbf{V}^\top)^{-1} = \mathbf{L}_2\mathbf{L}_1^{-1}, \\ \hat{\mathbf{Q}} &= \frac{(\mathbf{W} - \hat{\mathbf{G}}\mathbf{V})(\mathbf{W} - \hat{\mathbf{G}}\mathbf{V})^\top}{T - P - 1} = \frac{\mathbf{L}_3\mathbf{L}_3^\top}{T - P - 1}. \end{aligned} \quad (19)$$

D Connection to Existing Methods.

Given a one dimension time series $y \in \mathbb{R}^{T \times 1}$, which is modeled as a single-output Gaussian Process (GP) with kernel $\mathbf{K}(t, t')$. Current methods represent y as a stochastic differential equation (SDE) [Hartikainen & Särkkä, 2010]:

$$\frac{d^z y(t)}{dt^z} + a_{z-1} \frac{d^{z-1} y(t)}{dt^{z-1}} + \dots + a_1 \frac{y(t)}{dt} + a_0 y(t) = w(t), \quad (20)$$

where z is the order of derivatives, a_0, \dots, a_{z-1} are coefficients determined by the GP kernels and $w(t)$ is a white noise process. This SDE can further written as a continuous-time LDS:

$$\frac{dx(t)}{dt} = \mathbf{F}x(t) + \mathbf{L}w(t), \quad y(t) = \mathbf{H}x(t), \quad (21)$$

where $\mathbf{L} = [0, \dots, 0, 1]^\top \in \mathbb{R}^{z \times 1}$ is a constant vector, $\mathbf{H} = [1, 0, \dots, 0] \in \mathbb{R}^{1 \times z}$, and $\mathbf{F} \in \mathbb{R}^{z \times z}$ follows a controllable companion form [Grewal & Andrews, 2014]:

$$\mathbf{F} = \begin{bmatrix} 0 & 1 & & \\ & 0 & 1 & \\ & & \ddots & 1 \\ -a_0 & \dots & -a_{z-2} & -a_{z-1} \end{bmatrix}, \quad (22)$$

where a_0, \dots, a_{z-1} are scalar coefficients and \mathbf{F} has a similar structure with our transition matrix $\hat{\mathbf{A}}$ in Eq. 10, which follows a controller canonical form.

Then, the key is to notice that the spectral density $S(\omega)$ of kernel \mathbf{K} can be factorized into two parts:

$$\begin{aligned} S(\omega) &= \mathbf{G}(i\omega)q\mathbf{G}(-i\omega), \\ &= \mathbf{H}(\mathbf{F} + i\omega\mathbf{I})^{-1}\mathbf{L}q\mathbf{L}^\top[(\mathbf{F} - i\omega\mathbf{I})^{-1}]^\top\mathbf{H}^\top, \end{aligned} \quad (23)$$

where q is the spectral density of $w(t)$, which corresponds to the constant part in the kernel K , such as the amplitude σ^2 in the Squared Exponential kernel. This factorization can be computed using Spectral Factorization [Sayed & Kailath, 2001]. After we have \mathbf{F} , the next step is to convert the continuous-time LDS in Eq. 21 into a discrete-time form [Solin et al., 2016]:

$$x_t = \hat{\mathbf{F}}x_t + s_t, \quad s_t \sim \mathcal{N}(0, \mathbf{S}), \quad y(t) = \mathbf{H}x(t). \quad (24)$$

For multi-output separable kernels, e.g., Spatio-Temporal kernels, $\mathbf{K}_{st}(x, t) = \mathbf{K}_s(x, x')\mathbf{K}(t, t')$, we have:

$$\hat{\mathbf{F}}_{mo} = \mathbf{I} \otimes \hat{\mathbf{F}}, \quad \mathbf{S}_{mo} = \mathbf{K}_s \otimes \mathbf{S}. \quad (25)$$

For multi-output non-separable kernels with dimension M , the spectral density follows a matrix form $\mathbf{S}(\omega) \in \mathbb{R}^{M \times M}$, which can be factorized using Spectral Factorization (see Section 8.3.5 in [Kailath et al., 2000]). However, this factorization depends on the knowledge of the transition matrix and the measurement matrix. So, suppose we want to follow the methodology in single-output kernels. In that case, this creates a ‘‘chicken and egg’’ problem: the transition and measurement matrices are needed to perform spectral factorization, but spectral factorization is required to determine these matrices.

E Kalman Filter EM

In E-step, we have the expected log-likelihood as:

$$\begin{aligned}
Q(\Theta|\Theta^k) &= \mathbb{E}_{\mathbf{X} \sim p(\cdot|Y, \Theta^k)}[LL(\mathbf{X}, Y|\Theta)], \\
&\propto -\frac{1}{2} \sum_t (y_t^\top \mathbf{C}^{-1} y_t - 2y_t^\top \mathbf{C}^{-1} \mathbf{H} \mathbb{E}[x_t|Y, \Theta^k] + \mathbb{E}[x_t^\top \mathbf{H}^\top \mathbf{C}^{-1} \mathbf{H} x_t|Y, \Theta^k]) \\
&\quad -\frac{1}{2} \sum_t (\mathbb{E}[x_t^\top \hat{\mathbf{Q}}^{-1} x_t|Y, \Theta^k] - 2\mathbb{E}[x_t^\top \hat{\mathbf{Q}}^{-1} \hat{\mathbf{A}} x_{t-1}|Y, \Theta^k] \\
&\quad + \mathbb{E}[x_{t-1}^\top \hat{\mathbf{A}}^\top \hat{\mathbf{Q}}^{-1} \hat{\mathbf{A}} x_{t-1}|Y, \Theta^k]) - \frac{T}{2} \log(|\mathbf{C}|) - \frac{1}{2} \log(|\hat{\mathbf{Q}}|), \tag{26}
\end{aligned}$$

where all expectations $\mathbb{E}[\cdot]$ mentioned above are based on $\mathbb{E}[x_t|Y]$, $\mathbb{E}[x_t^\top x_t|Y]$, and $\mathbb{E}[x_t^\top x_{t-1}|Y]$, which are calculated through forward and backward passes known as Kalman Filtering and Kalman Smoothing [Boots, 2009], respectively. Specifically, if denoting $\tilde{x}_t = \mathbb{E}[x_t|Y]$, $\mathbf{C}_t = \mathbb{E}[x_t^\top x_t|Y]$, and $\mathbf{C}_{t,t-1} = \mathbb{E}[x_t^\top x_{t-1}|Y]$, we have:

$$\begin{aligned}
\mathbb{E}[x_t|Y, \Theta^k] &= \tilde{x}_t, \\
\mathbb{E}[x_t^\top \mathbf{H}^\top \mathbf{C}^{-1} \mathbf{H} x_t|Y, \Theta^k] &= \tilde{x}_t^\top \mathbf{H}^\top \mathbf{C}^{-1} \mathbf{H} \tilde{x}_t + \text{Tr}(\mathbf{H}^\top \mathbf{C}^{-1} \mathbf{H} \mathbf{C}_t), \\
\mathbb{E}[x_t^\top \hat{\mathbf{Q}}^{-1} x_t|Y, \Theta^k] &= \tilde{x}_t^\top \hat{\mathbf{Q}}^{-1} \tilde{x}_t + \text{Tr}(\hat{\mathbf{Q}}^{-1} \mathbf{C}_t), \\
\mathbb{E}[x_t^\top \hat{\mathbf{Q}}^{-1} \hat{\mathbf{A}} x_{t-1}|Y, \Theta^k] &= \tilde{x}_t^\top \hat{\mathbf{Q}}^{-1} \hat{\mathbf{A}} \tilde{x}_{t-1} + \text{Tr}(\hat{\mathbf{Q}}^{-1} \hat{\mathbf{A}} \mathbf{C}_{t,t-1}), \\
\mathbb{E}[x_{t-1}^\top \hat{\mathbf{A}}^\top \hat{\mathbf{Q}}^{-1} \hat{\mathbf{A}} x_{t-1}|Y, \Theta^k] &= \tilde{x}_{t-1}^\top \hat{\mathbf{A}}^\top \hat{\mathbf{Q}}^{-1} \hat{\mathbf{A}} \tilde{x}_{t-1} + \text{Tr}(\hat{\mathbf{A}}^\top \hat{\mathbf{Q}}^{-1} \hat{\mathbf{A}} \mathbf{C}_t).
\end{aligned} \tag{27}$$

Then, in M-step, we aim to update the parameters Θ such that $Q(\Theta|\Theta^k)$ is maximized:

$$\Theta^{k+1} = \arg \max_{\Theta} Q(\Theta|\Theta^k). \tag{28}$$

F Parameter Setting

- **Exponential (Exp)**: $P = 1, N = 2$.
- **Matern 3/2 (Matern)**: $P = 2, N = 2$.
- **Squared Exponential (SE)**: $P = 8, N = 2$.
- **Rational Quadratic (RQ)**: $P = 8, N = 2$.
- **Periodic**: $P = 6, N = 100$.
- **Spectral Mixture (SM)** [Wilson & Adams, 2013]: $P = 2, N = 3$.
- **Multi-Output Squared Exponential (MOSE)** [Gokcen et al., 2022]: $P = 2, N = 3$.
- **Multi-Output Spectral Mixture (MOSM)** [Parra & Tobar, 2017]: $P = 2, N = 3$.
- **Cross-Spectral Mixture (CSM)** [Ulrich et al., 2015]: $P = 4, N = 3$.
- **Linear Model of Coregionalization (LMC)**: When $k_q(t, t')$ is SE kernel, $P = 8, N = 3$.

For kernel parameters, amplitude $\alpha = 1$, length scale $l = 4.47$, $\alpha = 5$, $\omega = 0.5$ rad/s, the number of mixtures $Q = 2$, time delay $\delta = 2$, and phase delay $\phi = 1.0$.

G Training Details

All the experiments are performed on a Desktop with AMD 5800X CPU and NVIDIA RTX 3070 GPU.

For the methods (GP, SGPR, M-GP) in Section 5.2, the training consists of 100 epochs with an initial learning rate of 1.0, which decays by 0.1 every 25 iterations. We use the Adam optimizer for all methods. Then, the kernel hyperparameter $Q = 2$ is selected via 5-fold cross-validation for all methods, with no significant improvement observed when $Q \geq 2$. Since the signal-output kernel in LMC is SM kernel, the model hyperparameters P are set to the same values $P = 2$, and N is set to $N = 2$ as in Section 5.1.

For the methods (DLAG, M-GP) in Section 5.3, the training consists of 1000 epochs with a learning rate of 0.01, with DLAG implemented using the Autograd³ package. The optimizer for DLAG's M-step is L-BFGS, and the optimizer for M-GP's M-step is the Adam from Pytorch. For the neural data, we use neural spike train data (session 106r001p26, direction 0°) from V1 and V2 with 400 trials, each containing 64-time samples with a 20 ms bin size. We randomly select 300 trials as the training set and 100 trials as the testing set. To compare time cost in Figure 1(B), we change the bin size to create testing data with different time samples.

³<https://github.com/HIPS/autograd>

H DLAG Details

Given single region neural data $y^p \in \mathbb{R}^{n^p \times T}$, $p \in [1, \dots, P]$ is the brain region index, n^p denotes the number of neurons in region p , and T represents time steps.

DLAG aims to find the M independent low-dimensional variables $x^p \in \mathbb{R}^{M \times T}$ for each region's neural data y^p . These variables from P regions together form as $x = [x^1, \dots, x^P]^\top \in \mathbb{R}^{MP \times T}$, representing a latent representation for multi-region neural data $y = [y^1, \dots, y^P]^\top \in \mathbb{R}^{N \times T}$, where $N = n^1 + \dots + n^P$ is the total number of neurons over P regions.

Besides, y is a linear mapping of x : $y = \mathbf{L}x + d + \epsilon$, where \mathbf{L} is a block diagonal matrix $\mathbf{L} = \text{diag}\{\mathbf{L}^1, \dots, \mathbf{L}^p, \dots, \mathbf{L}^P\} \in \mathbb{R}^{N \times MP}$, $d \in \mathbb{R}^{N \times 1}$ is bias, and $\epsilon \sim \mathcal{N}(0, \mathbf{C})$ is Gaussian noise with $\mathbf{C} \in \mathbb{R}^{N \times N}$.

Meanwhile, DLAG assumes x^p can be split into across- and within-region parts [Gokcen et al., 2022]: $x^p = [x^{p,a}, x^{p,w}]^\top$, $x^{p,a} \in \mathbb{R}^{m_a \times T}$, $x^{p,w} \in \mathbb{R}^{m_w \times T}$, where m_a, m_w are the number of dimensions for across- or within-region part and $m_a + m_w = M$. Specifically, DLAG uses multi-output Squared Exponential kernel (MOSE) for across-region latent variables $x^{p,a}$, and single-output Squared Exponential kernels for within-region latent variables $x^{p,w}$.

The across-region variables $x^{p,a}$ describe neural activity that is shared across all brain regions, meaning that for the remaining $P - 1$ regions, they have the latent variables with the same dynamics except time delays, while the within-region variables $x^{p,w}$ describe the neural activity of region p that is not related to other regions.